IEEE Access
Multidisciplinary | Rapid Review | Open Access Journal

Received February 18, 2018, accepted March 30, 2018, date of publication April 23, 2018, date of current version May 9, 2018.

Digital Object Identifier 10.1109/ACCESS.2018.2828021

Ambient Backscatter Communication Systems: Capacity and Outage Performance Analysis

WENJING ZHAO[1], GONGPU WANG[1], RONGFEI FAN[2], LI-SHENG FAN[3], AND SAMAN ATAPATTU[4], (Member, IEEE)

[1]Beijing Key Lab of Transportation Data Analysis and Mining, School of Computer and Information Technology, Beijing Jiaotong University, Beijing 100044, China
[2]School of Information and Electronics, Beijing Institute of Technology, Beijing 100081, China
[3]School of Computer Science and Educational Software, Guangzhou University, Guangzhou 510006, China
[4]Department of Electrical and Electronic Engineering, The University of Melbourne, Melbourne, VIC 3010, Australia

Corresponding author: Gongpu Wang (gpwang@bjtu.edu.cn)

This work was supported in part by the Beijing Intelligent Logistics System Collaborative Innovation Center, in part by the National Natural Science Foundation of China (NSFC) under Grant 61571037, in part by NSFC Outstanding Youth under Grant 61725101, in part by the Fundamental Research Funds for the Central Universities under Grant 2016JBZ006, in part by the Key Laboratory of Universal Wireless Communications, Ministry of Education, China, under Grant KFKT-2018104, and in part by the Australian Research Council's Discovery Early Career Researcher Award under Grant DE160100020.

ABSTRACT Ambient backscatter is an emerging green communication technology that exploits the environmental radio frequency (RF) signals to enable passive devices to communicate with each other. This paper investigates channel capacity and outage performance of ambient backscatter communication systems. Specifically, a calculation method is proposed to facilitate capacity analysis, and the ambient backscatter system capacities are derived in the case of four different RF signals. It is surprisingly found that the channel capacity is obtained when the RF signals are not equiprobably backscattered by tag, and that the capacity with complex Gaussian RF signals is not exactly twice that with real ones for the ambient backscatter communication systems. Then, the outage probability and its asymptotic value in the high signal-to-noise ratio regime are obtained. Since the exact outage expression consists of an infinite number of terms, a tight truncation error bound is derived to reasonably estimate the number of effective terms for numerical simulation. Finally, simulation results are provided to corroborate theoretical analysis.

INDEX TERMS Ambient backscatter, channel capacity, Gaussian variable, Internet of Things, outage probability, performance analysis.

I. INTRODUCTION

Internet of Things (IoT), a vital component of the fifth generation (5G) mobile communications, aims to connect an enormous number of devices [1]. In practice, many devices such as tags and sensors, are usually powered by batteries. These devices restrict extensive IoT applications due to limited power supplies. Ambient backscatter, a new green communication technology, is suggested recently to provide a promising solution to the battery problem of IoT devices [2]–[4].

Ambient backscatter leverages environmental radio frequency (RF) signals such as digital television (TV) broadcasting, cellular or Wireless-Fidelity (Wi-Fi) signals as power and signal supplies to enable battery-less devices to harvest wireless energy and also to transmit information. Ambient backscatter can liberate sensors and tags from batteries, and thus eases manual maintenance such as recharging or replacement of batteries. Thus, it has good potential to be widely used in IoT, e.g., sensors located in dangerous spots filled with poisonous gases/liquids, or embedded inside building walls, and in the scenarios where wired communications are not convenient or available [5].

A typical ambient backscatter system consists of a reader and a tag. The communication process includes three steps: i) the tag harvests and stores wireless energy from ambient signals; ii) the tag separately indicates bit "1" or bit "0" by backscattering or absorbing the ambient signals; and iii) the reader decodes the backscattered signals and recovers the two states accordingly.

Recently, there arises a number of studies about ambient backscatter [6]. References [2]–[4] focus on hardware designs of the ambient backscatter prototypes that can enlarge

communication rates and coverage. Lu *et al.* [7] consider the device-to-device communications by integrating ambient backscatter. Several detection schemes for ambient backscatter communication systems are proposed in [8]–[10], and their corresponding bit error rate (BER) performance is analysed. Based on a differential encoder, a detector that avoids the knowledge of channel state information (CSI) is suggested in [9]. A joint-energy detection scheme is proposed in [10] that requires only channel variances rather than specific CSI. A successive interference cancellation (SIC) based detector and a maximum-likelihood (ML) detector with known CSI are presented in [8], to recover signals not only from readers but also from RF sources.

In addition, capacity and outage performance analysis for ambient backscatter communication systems are studied in [11]–[14]. Darsena *et al.* [11] analyse the channel capacity over orthogonal frequency division multiplexing (OFDM) signals. The ergodic capacity optimization problem at the reader with SIC is investigated by jointly considering the transmit source power and the reflection coefficient [12]. The BER of an energy detector is derived and the BER-based outage probability is obtained in [13] for ambient backscatter communication systems. In [14], the effective distribution of signal-to-noise ratio (SNR) is derived and the SNR-based outage probability is evaluated over real Gaussian channels.

However, existing capacity analysis in [12] and [15] are based on perfect SIC at the reader and certain signal processing at the tag. For many practical ambient backscatter communication systems, the tag can only realize binary modulation due to low wireless energy harvesting efficiency and simple design. For such case, the capacity of the ambient backscatter system remains an unknown issue [10] and the SNR-based outage performance over complex channels is also an open problem [13], [14], which motivates our current work.

In this paper, we investigate capacity and outage analysis of the ambient backscatter communication system with binary modulation at the tag in terms of mutual information[1] and outage probability. We first obtain probabilities of the received signals belonging to specified regions, and then calculate the mutual information of these received signals and tag signals. Subsequently, the channel capacity is obtained through maximizing the mutual information over the distribution of the signals modulated by the tag. Then, we study the outage probability over complex Gaussian channels, and analyse its asymptotic outage performance at high transmit SNR. Moreover, since the derived outage expression is the summation of infinite terms, the corresponding truncation error bound is calculated to ensure certain numerical accuracy requirements.

Our contributions are summarized as follows:

- The channel capacities of the ambient backscatter communication system with binary tag modulation are derived in the case of real or complex RF signals.
- The outage performance at the reader is evaluated, and the asymptotic outage probability at high SNR is obtained.
- Since the derived outage probability is the summation of infinite terms, the number of the truncation terms is suggested to facilitate numerical calculation and the corresponding truncation error bound is calculated.

[1] Some preliminary results were presented in [16].

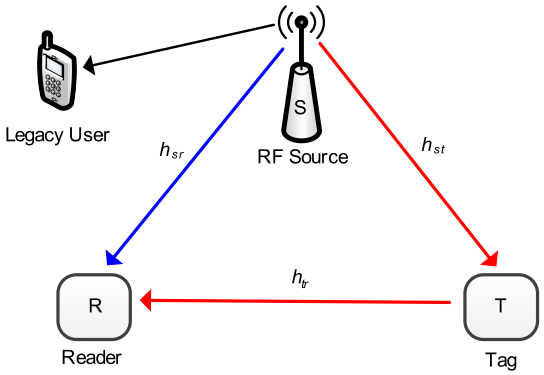

FIGURE 1. An ambient backscatter communication system.

The rest of the paper is organized as follows. Section II formulates the theoretical model of our ambient backscatter communication systems. Section III designs the method of capacity calculation targeting at real and complex Gaussian, binary phase-shift keying (BPSK), and M-ary phase-shift keying (MPSK) RF source signals, respectively. Section IV analyses the system outage performance as well as its asymptotic performance at high SNR. Section V provides numerical results. Section VI provides commendatory summaries.

Notations: $|h|$ is the modulus of variable h; $\mathcal{N}(\mu, \sigma^2)$ and $\mathcal{CN}(\mu, \sigma^2)$ individually denote real Gaussian distribution and circularly symmetric complex Gaussian (CSCG) distribution with mean μ and variance σ^2; $p(y|x)$ is the conditional probability of y given x; $\Re\mathfrak{e}X$ and $\Im\mathfrak{m}X$ represent the real part and the imaginary part of variable X, respectively.

II. SYSTEM MODEL

Consider an ambient backscatter communication system consisting of a reader (R) and a wireless-powered battery-less tag (T), as illustrated in Fig. 1. When RF source (S) broadcasts signals to its legacy users such as mobile phones and laptops, both the reader and the tag can also receive the RF signals. The tag first harvests energy from the RF signals, and then modulates its own information bit "1" or "0" over the RF signals by intentionally switching its antenna load coefficients [2] to backscatter the modulated signals to the reader or to absorb the signals inside the tag.

Denote the gains of the channels $S-R$, $S-T$ and $T-R$ as h_{sr}, h_{st} and h_{tr}, respectively. Represent $s(n)$ as the RF source signals with zero mean and unit variance. Assume transmit power of the RF source is P_s. The received signal at the tag can be then expressed as

$$y_t(n) = \sqrt{P_s} h_{st} s(n) + w_t(n), \tag{1}$$

where $w_t(n)$ is the noise inside the tag. Since the tag is a passive component, the noise inside the tag can be neglected, i.e., $w_t(n) \approx 0$ [2], [9].

Next the tag will modulate the received signal $y_t(n)$ with its own binary signal $x(n) \in \{0, 1\}$. Suppose probability $p(x(n) = i) = p_i$ for $i = 0, 1$. Clearly, $p_0 + p_1 = 1$. The signal backscattered by the tag is

$$x_t(n) = \eta x(n) y_t(n), \tag{2}$$

where $\eta \in [0, 1]$ is attenuation factor inside the tag. Accordingly, the signal received at the reader is

$$\begin{aligned} y_r(n) &= h_{sr} s(n) + h_{tr} x_t(n) + w(n) \\ &= \begin{cases} \sqrt{P_s} h_0 s(n) + w(n); & x(n) = 0, \\ \sqrt{P_s} h_1 s(n) + w(n); & x(n) = 1, \end{cases} \end{aligned} \tag{3}$$

where $h_0 \triangleq h_{sr}$, $h_1 \triangleq h_{sr} + \eta h_{st} h_{tr}$, and $w(n)$ is additive white Gaussian noise (AWGN) with zero mean and σ_w^2 variance.

III. CAPACITY ANALYSIS

The mutual information $I(X; Y)$ of two discrete random variables X and Y is defined as [17]

$$I(X; Y) = \sum_{x,y} p(x, y) \log_2 \frac{p(x, y)}{p(x) p(y)}, \tag{4}$$

where $p(x)$ and $p(y)$ are the probability mass functions of X and Y respectively, and $p(x, y)$ is the joint mass probability function of X and Y. The channel capacity is the maximum mutual information, i.e.,

$$C = \max_{p(x)} I(X; Y).$$

Clearly, the channel capacity for our ambient backscatter communication system is $\max_{p(x(n))} I(x(n); y_r(n))$, i.e., the maximum mutual information between $x(n)$ and $y_r(n)$. For brevity of our following discussion, we suppose $I(X; Y) = I(x(n); y_r(n))$ and we aim to derive $\max_{p_i} I(X; Y)$.

It can be readily observed that the tag signals are discrete while the signals received at the reader $y_r(n)$ in (3) are continuous. Therefore, the definition (4) cannot be directly applied to calculate the mutual information between $x(n)$ and $y_r(n)$. In addition, the capacity is closely related with the source signals $s(n)$. To address the two challenges, we first discuss four cases of the RF signals $s(n)$: i) real Gaussian signals; ii) complex Gaussian signals; iii) BPSK; and iv) MPSK. Then, compute the corresponding probabilities of the received signals $y_r(n)$ belonging to specified regions. Next we derive the mutual information $I(X; Y)$, from which the channel capacity is obtained.

A. CHANNEL CAPACITY WITH REAL GAUSSIAN SIGNALS

This subsection aims to obtain the channel capacity $C_{\text{Real}} = \max_{p_i} I(X; Y)$ in the case of $s(n) \sim \mathcal{N}(0, 1)$ and

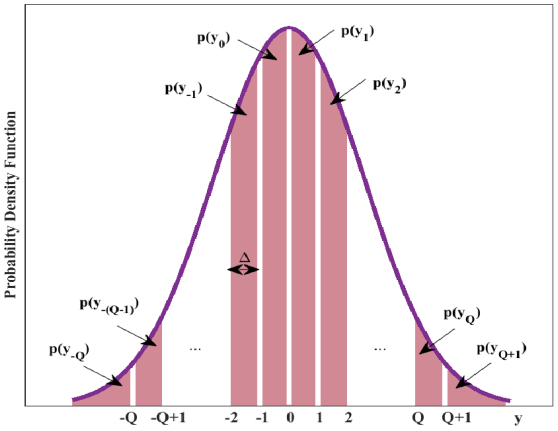

FIGURE 2. Region partition for probability calculation of real Gaussian variable.

$w(n) \sim \mathcal{N}(0, \sigma_w^2)$. In such case, we have

$$y_r(n) \sim \begin{cases} \mathcal{N}(0, \sigma_0^2); & x(n) = 0, \\ \mathcal{N}(0, \sigma_1^2); & x(n) = 1, \end{cases} \tag{5}$$

where $\sigma_0^2 \triangleq |h_0|^2 P_s + \sigma_w^2$ and $\sigma_1^2 \triangleq |h_1|^2 P_s + \sigma_w^2$.

We divide the continuous signals $y_r(n)$ in the case of $x(n) = i \in \{0, 1\}$ into $2(Q + 1)$ intervals through the following steps as shown in Fig. 2:

1) The interval $[0, \infty)$ of the horizontal axis is divided into $Q + 1$ subintervals, and the interval length of the first Q subintervals is set as Δ;
2) For given $x(n) = i$, the probabilities of $y_q \in [(q - 1)\Delta, q\Delta]$ for $q = 1, 2, \cdots, Q$ and $y_{Q+1} \in [Q\Delta, \infty)$ is computed;
3) Similar steps are carried out for the interval $(-\infty, 0)$.

Utilizing Bayes Rule, the mutual information $I(X; Y)$ in (4) can be given as

$$I(X; Y) = \sum_{i \in \{0,1\}} p_i \sum_{q=-Q}^{Q+1} p(y_q|i) \log_2 \frac{p(y_q|i)}{\sum_{i \in \{0,1\}} p(y_q|i) p_i}. \tag{6}$$

Due to the symmetry of Gaussian probability distribution function (5), the mutual information (6) can be rewritten as

$$I(X; Y) = 2 \sum_{i \in \{0,1\}} p_i \sum_{q=1}^{Q+1} p(y_q|i) \log_2 \frac{p(y_q|i)}{\sum_{i \in \{0,1\}} p(y_q|i) p_i}. \tag{7}$$

The probabilities $p(y_q|i)$ for $q = 1, \cdots, Q$ and $p(y_{Q+1}|i)$ can be calculated as

$$\begin{aligned} p(y_q|i) &= \int_{(q-1)\Delta}^{q\Delta} \frac{1}{\sqrt{2\pi\sigma_i^2}} e^{-\frac{z^2}{2\sigma_i^2}} dz \\ &= \frac{1}{2} \Phi\left(\frac{q\Delta}{\sqrt{2\sigma_i^2}}\right) - \frac{1}{2} \Phi\left(\frac{(q-1)\Delta}{\sqrt{2\sigma_i^2}}\right), \end{aligned} \tag{8}$$

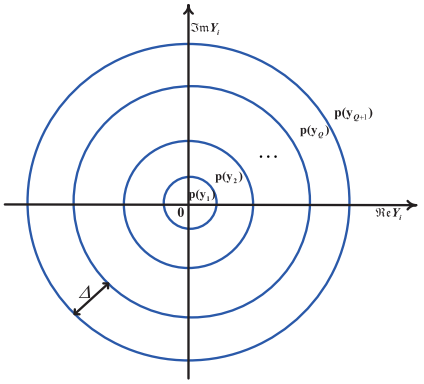

FIGURE 3. Region partition for probability calculation of complex Gaussian variable.

and

$$p(y_{Q+1}|i) = \frac{1}{2} - \frac{1}{2}\Phi\left(\frac{Q\Delta}{\sqrt{2\sigma_i^2}}\right), \tag{9}$$

where the probability integral function $\Phi(\cdot)$ [18, eq. (8.250.1)] is defined as

$$\Phi(x) = \frac{2}{\sqrt{\pi}}\int_0^x e^{-t^2}dt.$$

As the number of terms Q tends to infinity, i.e., $Q \to \infty$, the interval length Δ approaches zero. As a result, the terms containing $p(y_{Q+1}|i)$ in (7) approximate to zero, i.e.,

$$p_0\, p(y_{Q+1}|0)\log_2 \frac{p(y_{Q+1}|0)}{p_0\, p(y_{Q+1}|0)+(1-p_0)p(y_{Q+1}|1)} \approx 0,$$

and

$$(1-p_0)p(y_{Q+1}|1) \times \log_2 \frac{p(y_{Q+1}|1)}{p_0\, p(y_{Q+1}|0) + (1-p_0)p(y_{Q+1}|1)} \approx 0.$$

The mutual information in (7) can be further obtained as

$$I(X;Y) = 2\sum_{i\in\{0,1\}} p_i \sum_{q=1}^{Q} p(y_q|i)\log_2 \frac{p(y_q|i)}{\sum\limits_{i\in\{0,1\}} p(y_q|i)p_i}. \tag{10}$$

B. CHANNEL CAPACITY WITH COMPLEX GAUSSIAN SIGNALS

This subsection studies the channel capacity $C_{\text{Complex}} = \max\limits_{p_i} I(X;Y)$ in the case of $s(n) \sim \mathcal{CN}(0,1)$ and $w(n) \sim \mathcal{CN}(0,\sigma_w^2)$. In such case, we have

$$y_r(n) \sim \begin{cases} \mathcal{CN}(0,\sigma_0^2); & x(n)=0, \\ \mathcal{CN}(0,\sigma_1^2); & x(n)=1. \end{cases} \tag{11}$$

As shown in Fig. 3, we take the following steps to divide the continuous complex signals $y_r(n)$ in the case of $x(n) = i \in \{0,1\}$ into $Q+1$ intervals:

1) The complex plane is divided into Q concentric circles with center $(0,0)$;
2) The radius difference between the adjacent circles in Fig. 3 is set as Δ;
3) Let y_q belong to the region between the $(q-1)$th circle and the qth circle for $q = 1, 2, \cdots, Q$, and let y_{Q+1} belong to the remaining region.

Considering that the real and imaginary parts of $y_r(n)$ are independent and identically distributed (i.i.d.) for given $x(n) = i$, the mutual information $I(X;Y)$ can be obtained as

$$I(X;Y) = \sum_{i\in\{0,1\}} p_i \sum_{q=1}^{Q+1} p(y_q|i)\log \frac{p(y_q|i)}{\sum\limits_{i\in\{0,1\}} p(y_q|i)p_i}, \tag{12}$$

where, for $q = 1, \cdots, Q$, we have

$$p(y_q|i) = \int_{(q-1)\Delta}^{q\Delta} \frac{2z}{\sigma_i^2} e^{-\frac{z^2}{\sigma_i^2}} dz = e^{-\frac{(q-1)^2\Delta^2}{\sigma_i^2}} - e^{-\frac{q^2\Delta^2}{\sigma_i^2}}, \tag{13}$$

$$p(y_{Q+1}|i) = \int_{Q\Delta}^{\infty} \frac{2z}{\sigma_i^2} e^{-\frac{z^2}{\sigma_i^2}} dz = e^{-\frac{Q^2\Delta^2}{\sigma_i^2}}. \tag{14}$$

Theorem 1: When the signals received at the reader Y are CSCG distributed, the mutual information between the tag and reader signals X and Y is equivalent to that between the signals X and the modulus of the signals Y, i.e.,

$$I(X;Y) = I(X;|Y|). \tag{15}$$

The proof is in Appendix VI-A.

C. CHANNEL CAPACITY WITH BPSK SIGNALS

This subsection investigates the channel capacity $C_{\text{BPSK}} = \max\limits_{p_i} I(X;Y)$ with $w(n) \sim \mathcal{N}(0,\sigma_w^2)$. Suppose the RF source transmits BPSK signals $s(n) \in \{-1,1\}$, and we can obtain

$$y_r(n) \sim \begin{cases} \mathcal{N}(\sqrt{P_s}h_0, \sigma_w^2); & s(n)=1, x(n)=0, \\ \mathcal{N}(-\sqrt{P_s}h_0, \sigma_w^2); & s(n)=-1, x(n)=0, \\ \mathcal{N}(\sqrt{P_s}h_1, \sigma_w^2); & s(n)=1, x(n)=1, \\ \mathcal{N}(-\sqrt{P_s}h_1, \sigma_w^2); & s(n)=-1, x(n)=1. \end{cases} \tag{16}$$

Then, the probability density function (PDF) of $y_r(n)$ for given $x(n) = i$, denoted as $f_{Y|i}(y)$, can be given as

$$f_{Y|i}(y) = \frac{\lambda}{\sqrt{2\pi\sigma_w^2}} e^{-\frac{(y-\sqrt{P_s}h_i)^2}{2\sigma_w^2}} + \frac{1-\lambda}{\sqrt{2\pi\sigma_w^2}} e^{-\frac{(y+\sqrt{P_s}h_i)^2}{2\sigma_w^2}}, \tag{17}$$

where λ and $1-\lambda$ are the probabilities of transmitting signals $s(n) = 1$ and $s(n) = -1$, respectively.

Taking similar steps as shown in Section III-A, the corresponding probabilities $p(y_q|i)$ for $q = -Q+1, 2, \cdots, Q$,

$p(y_{-Q}|i)$, and $p(y_{Q+1}|i)$ can be computed as

$$\begin{aligned} &p(y_q|i) \\ &= \int_{(q-1)\Delta}^{q\Delta} \frac{\lambda}{\sqrt{2\pi\sigma_w^2}} e^{-\frac{(y-\sqrt{P_s}h_i)^2}{2\sigma_w^2}} + \frac{1-\lambda}{\sqrt{2\pi\sigma_w^2}} e^{-\frac{(y+\sqrt{P_s}h_i)^2}{2\sigma_w^2}} dy \\ &= \frac{\lambda}{2}\left[\Phi\left(\frac{q\Delta-\sqrt{P_s}h_i}{\sqrt{2\sigma_w^2}}\right) - \Phi\left(\frac{(q-1)\Delta-\sqrt{P_s}h_i}{\sqrt{2\sigma_w^2}}\right)\right] \\ &\quad + \frac{1-\lambda}{2}\left[\Phi\left(\frac{q\Delta+\sqrt{P_s}h_i}{\sqrt{2\sigma_w^2}}\right) - \Phi\left(\frac{(q-1)\Delta+\sqrt{P_s}h_i}{\sqrt{2\sigma_w^2}}\right)\right], \end{aligned} \tag{18}$$

$$\begin{aligned} p(y_{-Q}|i) = 1 &- \frac{\lambda}{2}\Phi\left(\frac{Q\Delta+\sqrt{P_s}h_i}{\sqrt{2\sigma_w^2}}\right) \\ &- \frac{1-\lambda}{2}\Phi\left(\frac{Q\Delta-\sqrt{P_s}h_i}{\sqrt{2\sigma_w^2}}\right), \end{aligned} \tag{19}$$

and

$$\begin{aligned} p(y_{Q+1}|i) = 1 &- \frac{\lambda}{2}\Phi\left(\frac{Q\Delta-\sqrt{P_s}h_i}{\sqrt{2\sigma_w^2}}\right) \\ &- \frac{1-\lambda}{2}\Phi\left(\frac{Q\Delta+\sqrt{P_s}h_i}{\sqrt{2\sigma_w^2}}\right). \end{aligned} \tag{20}$$

Then, substituting (18), (19), and (20) into (6) yields the mutual information over real channels with BPSK signals.

D. CHANNEL CAPACITY WITH MPSK SIGNALS

This subsection investigates the channel capacity $C_{\text{MPSK}} = \max_{p_i} I(X;Y)$ in the case of MPSK signals $s(n)$ and complex AWGN $w(n)$. In such case, we have

$$y_r(n) \sim \mathcal{CN}(\mu_{i,m}, \sigma_w^2); \quad s(n) = e^{j\frac{2\pi(m-1)}{M}}, x(n) = i, \tag{21}$$

where $\mu_{i,m} = \sqrt{P_s}h_i e^{j\frac{2\pi(m-1)}{M}}$, $m \in \{1, 2, \cdots, M\}$ and $M \in \{2, 4, 8, \cdots\}$ is the MPSK modulation phase number.

Then the PDF $f_{Y|i}(y)$ can be expressed as

$$f_{Y|i}(y) = \sum_{m=1}^{M} \frac{\lambda_m}{\pi\sigma_w^2} e^{-\frac{|y-\sqrt{P_s}h_i e^{j\frac{2\pi(m-1)}{M}}|^2}{\sigma_w^2}}, \tag{22}$$

where λ_m denotes the probability of transmitting signal $s(n) = e^{j\frac{2\pi(m-1)}{M}}$, and $\sum_{m=1}^{M}\lambda_m = 1$. Taking similar steps in Section III-B, the mutual information in (12) can be reformulated by replacing $p(y_q|i)$ for $q = 1, 2, \cdots, Q$ and $p(y_{Q+1}|i)$, respectively, with

$$\begin{aligned} p(y_q|i) &= \int_{(q-1)\Delta}^{q\Delta} f_{Y|i}(y)dy \\ &= \sum_{k=0}^{\infty} \frac{|h_i|^{2k}P_s^k e^{-\frac{|h_i|^2P_s}{\sigma_w^2}}}{(\sigma_w^2)^k(k!)^2}\left[\gamma\left(k+1, \frac{q^2\Delta^2}{\sigma_w^2}\right)\right. \\ &\quad \left. -\gamma\left(k+1, \frac{(q-1)^2\Delta^2}{\sigma_w^2}\right)\right], \end{aligned} \tag{23}$$

and

$$p(y_{Q+1}|i) = 1 - \sum_{k=0}^{\infty} \frac{|h_i|^{2k}P_s^k e^{-\frac{|h_i|^2P_s}{\sigma_w^2}} \gamma\left(k+1, \frac{Q^2\Delta^2}{\sigma_w^2}\right)}{(\sigma_w^2)^k(k!)^2}. \tag{24}$$

The proof is in Appendix B.

Remark 1: Equations (23) and (24) indicate that the channel capacity C_{MPSK} in the case of MPSK signals is unrelated to the MPSK modulation phase number M.

IV. OUTAGE ANALYSIS

In this section, we investigate the outage performance and its asymptotic value in the high SNR regime. We derive the outage probability that contains infinite terms, truncate it to reduce the computational complexity, and obtain the corresponding truncation error.

A. EFFECTIVE SNR DISTRIBUTION

The PDF of the channel modulus $|h|$, $f_{|h|}(x)$, can be derived as [19]

$$f_{|h|}(x) = \begin{cases} \frac{2x}{\sigma_{sr}^2} e^{-\frac{x^2}{\sigma_{sr}^2}}; & x(n) = 0, \\ \sum_{m=0}^{\infty} \frac{x^{2m+1}}{\sigma_{sr}^{2m+1}} W_{-m-\frac{1}{2},0}(2\nu) & \\ \quad \times \frac{2}{\sqrt{\eta^2\sigma_{st}^2\sigma_{tr}^2}} e^{\nu-\frac{x^2}{\sigma_{sr}^2}}; & x(n) = 1, \end{cases} \tag{25}$$

where $\nu = \frac{\sigma_{sr}^2}{2\eta^2\sigma_{st}^2\sigma_{tr}^2}$, and Whittaker function $W_{\lambda,\mu}(\cdot)$ is defined as [18, eq. (9.223)]

$$\begin{aligned} W_{\lambda,\mu}(z) = \frac{e^{-\frac{\pi}{2}}}{2\pi i}\int_{-i\infty}^{i\infty} &\frac{\Gamma(u-\lambda)\Gamma(-u-\mu+\frac{1}{2})}{\Gamma(-\lambda+\mu+\frac{1}{2})\Gamma(-\lambda-\mu+\frac{1}{2})} \\ &\times\Gamma(-u+\mu+\frac{1}{2})z^u du. \end{aligned}$$

The receive SNR at the reader is $\rho = \bar{\rho}|h|^2$ with average transmit SNR $\bar{\rho} = \frac{P_s}{\sigma_w^2}$. After a linear variable conversion for (25), the PDF of ρ, $f_\rho(x)$, can be derived as

$$f_\rho(x) = \frac{f_{|h|}\left(\sqrt{\frac{x}{\bar{\rho}}}\right)}{2\sqrt{\bar{\rho}x}}. \tag{26}$$

B. OUTAGE PROBABILITY

Outage occurs when the SNR at the reader falls below a certain predetermined threshold ρ_t [20]. Thus, the outage probability can be expressed as

$$P_o = \Pr[\rho \le \rho_t] = \int_0^{\rho_t} f_\rho(x)dx = p_0P_{o|0} + p_1P_{o|1}, \tag{27}$$

where $P_{o|i}$ is the outage probability for given $x(n) = i$ which can be derived as

$$P_{o|0} = 1 - e^{-\frac{\rho_t}{\bar{\rho}\sigma_{sr}^2}}, \tag{28}$$

$$P_{o|1} = \sqrt{2\nu}e^{\nu}\sum_{m=0}^{\infty} W_{-m-\frac{1}{2},0}(2\nu)\gamma\left(m+1, \frac{\rho_t}{\bar{\rho}\sigma_{sr}^2}\right), \tag{29}$$

where (29) can be obtained with the aid of the integral representation of incomplete gamma function $\gamma(\cdot,\cdot)$ [18, eq. (8.350.1)].

C. ASYMPTOTIC ANALYSIS FOR HIGH SNR

At high SNR, the outage of the reader is approximated as

$$P_o^{\infty} = p_0 P_{o|0}^{\infty} + p_1 P_{o|1}^{\infty}, \tag{30}$$

where $P_{o|i}^{\infty}$ is the asymptotic probability in the case of $x(n) = i$, which can be derived as

$$P_{o|0}^{\infty} = \frac{\rho_t}{\sigma_{sr}^2}\frac{1}{\bar{\rho}} \text{ and } P_{o|1}^{\infty} = \sqrt{2\nu}e^{\nu}W_{-\frac{1}{2},0}(2\nu)\frac{\rho_t}{\sigma_{sr}^2}\frac{1}{\bar{\rho}}.$$

The proof is in Appendix C. Since the diversity order is conventionally defined as $d = -\lim_{\bar{\rho}\to\infty}\frac{\log P_o}{\log \bar{\rho}}$, ambient backscatter communication system can attain diversity order of 1 over complex Gaussian channels, which is exactly twice of that over real ones [14]. This relationship is in conformity with that in traditional point-to-point systems.

D. TRUNCATION ERROR BOUND

Noting that the outage probability (29) in the case of $x(n) = 1$ comprises of an infinite number of terms. We therefore truncate it with finite terms (i.e., its first T terms) to facilitate numerical evaluation (29). The truncation error $|\epsilon_T|$ can be bounded as

$$|\epsilon_T| \le \frac{2\nu\Psi(1,1;2\nu)}{T!}\left[\frac{\rho_t}{\sigma_{sr}^2\bar{\rho}}\gamma\left(T+1,\frac{\rho_t}{\sigma_{sr}^2\bar{\rho}}\right) - \gamma\left(T+2,\frac{\rho_t}{\sigma_{sr}^2\bar{\rho}}\right)\right], \tag{31}$$

where $\Psi(\cdot,\cdot,\cdot)$ is the confluent hypergeometric function [18, eq. (9.211.4)]. The proof is in Appendix D.

V. NUMERICAL AND SIMULATION RESULTS

In this section, we numerically evaluate the capacity and the outage performance.

A. NUMERICAL RESULTS OF THE CHANNEL CAPACITY

Throughout this subsection, channel gains are set as $h_{sr} = 0.2916$, $h_{st} = 0.1978$ and $h_{tr} = 2.7500$[2]; the attenuation factors are configured with $\eta = 0.3$ and $\eta = 0.7$. Additionally, the interval length is chosen as $\Delta = 0.026$ for the MPSK RF signals, and $\Delta = 0.031$ for the other RF signals.

Fig. 4 displays the mutual information $I(X;Y)$ versus the number of intervals Q in the case of the MPSK RF signals with average transmit SNR $\bar{\rho} = 20$ dB. It can be seen that the maxima are equal when $\Delta = 0.026$ and $\Delta = 0.031$, respectively, which indicates that the maximum of the mutual information is not affected by the interval length and can be obtained just by a reasonable interval. Thus, we can choose the interval length Δ as 0.026 for the scenario with MPSK signals, which proves the rationality of our parameter settings.

[2]The channel gains do not affect the trends of the curves in the simulation results.

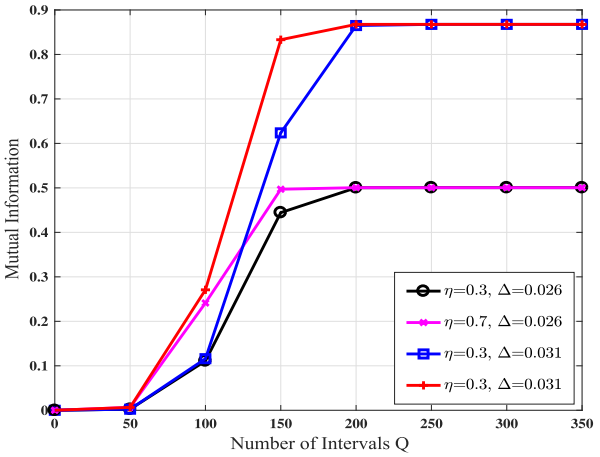

FIGURE 4. Mutual information $I(X;Y)$ versus number of intervals Q when RF source transmits MPSK signals.

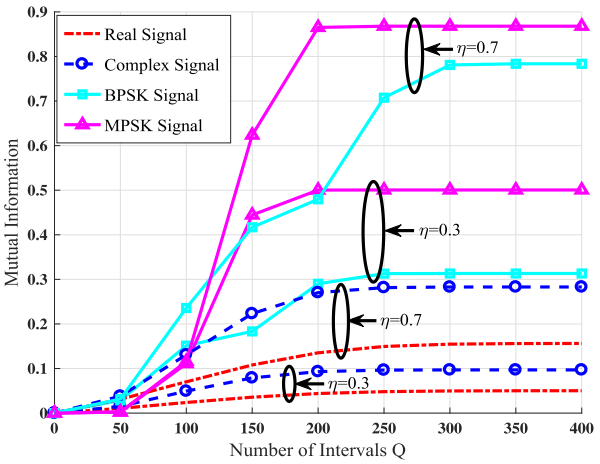

FIGURE 5. Mutual information $I(X;Y)$ versus number of intervals Q.

Fig. 5 shows the mutual information $I(X;Y)$ versus the number of intervals Q when average transmit SNR $\bar{\rho} = 20$ dB. With the number of intervals growing, the mutual information gradually increases and finally remains unchanged. Consequently, it is well-justified to choose $Q = 400$ when SNR $= 20$ dB. Fig. 6 illustrates the mutual information $I(X;Y)$ versus the probability p_0 in case of real Gaussian, complex Gaussian, BPSK and MPSK signals with average transmit SNR $\bar{\rho} = 20$ dB, respectively. The maxima in Fig. 6 are exactly the channel capacities under the corresponding constraints. As shown in Fig. 6, the mutual information $I(X;Y)$ first witnesses an upward trend and then falls consistently when increasing probability p_0. Besides, an lower attenuation factor η results in an reduced mutual information $I(X;Y)$. It can be also found that the extreme point of the mutual information $I(X;Y)$ is not identically 0.5, which indicates that the ambient backscatter channel capacity is achieved when the tag signals $x(n)$ are not equiprobable.

Fig. 7 depicts the channel capacity versus the average transmit SNR. The channel capacity can be obtained by

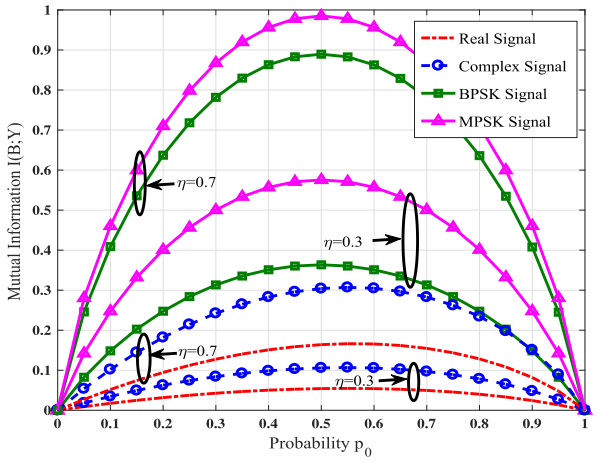

FIGURE 6. Mutual information $I(X;Y)$ versus probability p_0.

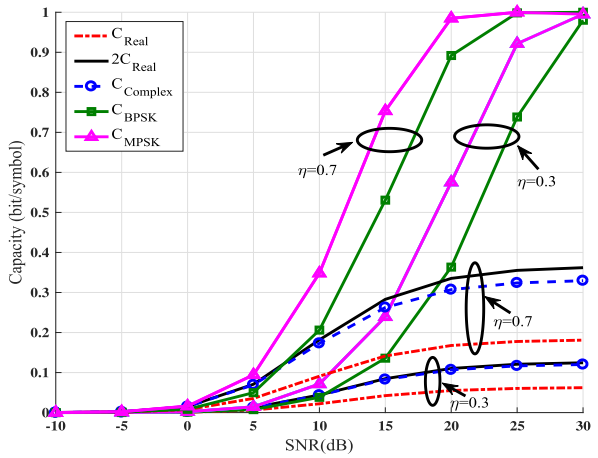

FIGURE 7. Capacity versus SNR.

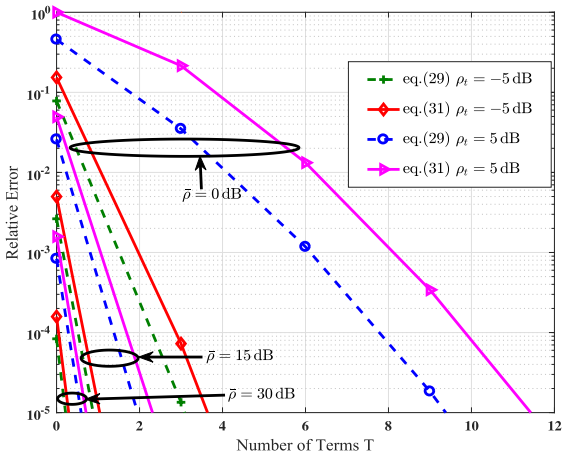

FIGURE 8. Relative error versus number of terms T.

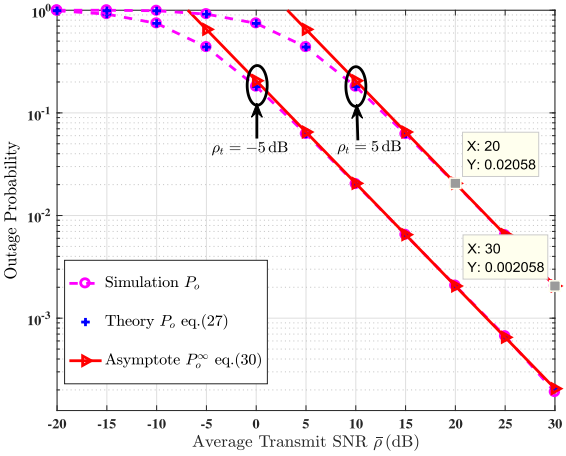

FIGURE 9. Outage probability versus average transmit SNR $\bar{\rho}$.

maximizing the corresponding mutual information $I(X;Y)$ over the distribution of tag signals $x(n)$. It can be seen in Fig. 7 that the channel capacity increases when enlarging transmit SNR and approaches a ceiling at high SNR. It can also be found that the capacity performance with MPSK/BPSK signals is better than that with complex/real Gaussian signals under same transmit SNR, which is in accordance with the results in Fig. 7. Additionally, different from a traditional point-to-point communication system, the capacity with complex Gaussian signals is not always twice that with real ones.

B. NUMERICAL RESULTS OF THE SYSTEM OUTAGE

In this subsection, we set $p_0 = \frac{1}{2}$ and $\eta = 0.7$, and consider two thresholds $\rho_t = -5\,\text{dB}$ and $\rho_t = 5\,\text{dB}$. In most practical situations, since the distance between the RF source and the reader, and the distance between the RF source and the tag are much greater than the distance between the reader and the tag [2], we choose $\sigma_{sr}^2 = 1$, $\sigma_{st}^2 = 2$ and $\sigma_{tr}^2 = 5$.

When $x(n) = 1$, we first calculate the truncation error bound (31). Next we calculate the relative error with truncation as $\frac{|\text{exact}-\text{truncated}|}{\text{exact}}$, the relative error with bound as $\frac{\text{error bound in (31)}}{\text{exact value}}$, the exact value with numerical integration, and the truncated value for different T by using (29).

Fig. 8 illustrates the relative error versus the number of terms T with different average transmit SNRs. Given $\rho_t = 5\,\text{dB}$, both the relative error with truncation and that with bound are less than 10^{-4} when $T \geq 2$ and $T \geq 1$ for $\bar{\rho} = 15\,\text{dB}$ and $\bar{\rho} = 30\,\text{dB}$, respectively. While for $\rho_t = 5\,\text{dB}$ and $\bar{\rho} = 0\,\text{dB}$, the relative error with truncation and that with bound are less than 10^{-4} when $T \geq 8$ and $T \geq 10$ separately. These demonstrate the tightness of our error bound (31). Moreover, Fig. 8 also shows that a very accurate outage value can be calculated by using small T.

Fig. 9 depicts the outage probabilities (27) and (30) versus the average transmit SNR $\bar{\rho}$. It can be found that increasing $\bar{\rho}$ reduces the outage probabilities, and that the asymptotic expression (30) also approaches the exact value (27) in the high SNR regime. For any two points (x_1, y_1) and (x_2, y_2) on the same asymptote in Fig. 9, we can compute the slope of the asymptote as -1 by $\frac{\log(y_1)-\log(y_2)}{\log(10^{\frac{x_1}{10}})-\log(10^{\frac{x_2}{10}})}$, $\frac{\log(0.02058)-\log(0.002058)}{\log(10^{\frac{20}{10}})-\log(10^{\frac{30}{10}})}$ for example, which coincides with the diversity order analysis in Section IV-C.

VI. CONCLUSION

This paper investigated the capacity and outage performance of ambient backscatter communication systems. We first developed a method to facilitate capacity analysis and then found the system capacities in four cases of different RF source signals. It was surprisingly found that the channel capacity was achieved when the RF signals were not equiprobably backscattered by the tag, and that the capacity with complex Gaussian signals was not exactly twice that with real Gaussian ones. Our simulation results further disclosed that MPSK/BPSK RF signals could achieve larger channel capacity than complex/real Gaussian signals. We next derived the outage probability in closed form. Since the outage probability contains infinite terms, we obtained its asymptotic outage at high SNR and truncation error bound. It was found that the asymptotic outage probability could well approach the exact value, and our truncation error bound could provide a reasonable estimation for the number of the truncation terms.

APPENDIX

A. PROOF OF THEOREM 1

Denote $y_r(n)$ under $x(n) = i$ in (11) as Y_i. Due to the independence between $\Re\mathrm{e}Y_i$ and $\Im\mathrm{m}Y_i$, the PDF of Y_i is

$$f(\Re\mathrm{e}Y_i, \Im\mathrm{m}Y_i) = \frac{e^{-\frac{(\Re\mathrm{e}Y_i)^2+(\Im\mathrm{m}Y_i)^2}{\sigma_i^2}}}{\pi\sigma_i^2} = \frac{1}{\pi\sigma_i^2} e^{-\frac{|Y_i|^2}{\sigma_i^2}}. \quad \text{(A.1)}$$

Further, the probability of y_q for given $x(n) = i$ can be expressed as

$$\begin{aligned} p(y_q|i) &= \int\int_D f(\Re\mathrm{e}Y_i, \Im\mathrm{m}Y_i) d\Re\mathrm{e}Y_i d\Im\mathrm{m}Y_i \\ &\overset{(a)}{=} \int_0^{2\pi}\int_{(q-1)\Delta}^{q\Delta} f(|Y_i|\cos\theta, |Y_i|\sin\theta)|Y_i| d|Y_i| d\theta \\ &\overset{(b)}{=} \int_0^{2\pi}\int_{(q-1)\Delta}^{q\Delta} \frac{1}{\pi\sigma_i^2} e^{-\frac{|Y_i|^2}{\sigma_i^2}} |Y_i| d|Y_i| d\theta \\ &= \int_{(q-1)\Delta}^{q\Delta} \frac{2|Y_i|}{\sigma_i^2} e^{-\frac{|Y_i|^2}{\sigma_i^2}} d|Y_i|, \end{aligned} \quad \text{(A.2)}$$

where (a) is obtained by converting to polar coordinates, and (b) is gained through the substitution of (A.1). Apparently, the integral function in (A.2) is the expression of Rayleigh distribution, which is exactly the PDF of $|y_r(n)|$ for given $x(n) = i$.

B. PROOF OF (23) and (24)

According to (22), the PDF of $z = |y|$ is

$$f_{Z|i}(z) = \sum_{m=1}^{M} \frac{2\lambda_m z}{\sigma_w^2} e^{-\frac{z^2+|\mu_{i,m}|^2}{\sigma_w^2}} I_0\left(\frac{2|\mu_{i,m}|z}{\sigma_w^2}\right), \quad \text{(B.1)}$$

where $|\mu_{i,m}| = \sqrt{P_s}|h_i|$ and the modified Bessel functions of the first kind $I_\nu(\cdot)$ is defined as

$$I_\nu(z) = \sum_{k=0}^{\infty} \frac{1}{k!\Gamma(\nu+k+1)} \left(\frac{z}{2}\right)^{\nu+2k}. \quad \text{(B.2)}$$

By expanding $I_\nu(\cdot)$ with its series as shown in (B.2), eq. (B.1) can be further rewritten as

$$\begin{aligned} f_{Z|i}(z) &= \sum_{m=1}^{M}\sum_{k=0}^{\infty} \frac{2\lambda_m|\mu_{i,m}|^{2k}}{(\sigma_w^2)^{2k+1}(k!)^2} e^{-\frac{|\mu_{i,m}|^2}{\sigma_w^2}} z^{2k+1} e^{-\frac{z^2}{\sigma_w^2}} \\ &= \sum_{k=0}^{\infty} \frac{2|\mu_{i,m}|^{2k}}{(\sigma_w^2)^{2k+1}(k!)^2} e^{-\frac{|\mu_{i,m}|^2}{\sigma_w^2}} z^{2k+1} e^{-\frac{z^2}{\sigma_w^2}}. \end{aligned} \quad \text{(B.3)}$$

Based on (B.3), the probability $p(y_q|i)$ for $q = 1, 2, \cdots, Q$ can be calculated as $p(y_q|i) = \int_{(q-1)\Delta}^{q\Delta} f_{Z|i}(z)dz$, which results

$$p(y_q|i) = \sum_{k=0}^{\infty} \frac{2|\mu_{i,m}|^{2k} e^{-\frac{|\mu_{i,m}|^2}{\sigma_w^2}}}{(\sigma_w^2)^{2k+1}(k!)^2} \int_{(q-1)\Delta}^{q\Delta} z^{2k+1} e^{-\frac{z^2}{\sigma_w^2}} dz. \quad \text{(B.4)}$$

Similarly, the probability $p(y_{Q+1}|i)$ can be computed as

$$p(y_{Q+1}|i) = 1 - \sum_{k=0}^{\infty} \frac{2|\mu_{i,m}|^{2k} e^{-\frac{|\mu_{i,m}|^2}{\sigma_w^2}}}{(\sigma_w^2)^{2k+1}(k!)^2} \int_{0}^{Q\Delta} z^{2k+1} e^{-\frac{z^2}{\sigma_w^2}} dz. \quad \text{(B.5)}$$

According to [18, eq. (3.381.8)], the results of (B.4) and (B.5) are given by (23) and (24), respectively.

C. PROOF OF (30)

In the case of $x(n) = 0$ and using series representation of the error function erf(·) [18, eq. (8.253.1)], eq. (28) can be expanded as

$$1 - e^{-\frac{\rho_t}{\bar{\rho}\sigma_{sr}^2}} = 1 - \sum_{k=0}^{\infty} \frac{(-1)^k \rho_t^k}{\bar{\rho}^k \sigma_{sr}^{2k} k!}.$$

When $\bar{\rho} \to \infty$, we consider the lowest exponent for $1/\bar{\rho}$, i.e., the index $k = 0$. Similarly, in the case of $x(n) = 1$, incomplete gamma function $\gamma(\cdot,\cdot)$ in (29) can be expanded as

$$\gamma(a, x) = \sum_{j=0}^{\infty} \frac{(-1)^j x^{a+j}}{j!(a+j)}.$$

We then consider the lowest exponent for $1/\bar{\rho}$, i.e., the indies $k = 0$ and $j = 0$. Thereby, when the average transmit SNR goes to infinity, namely, $\bar{\rho} \to \infty$, a simplified outage probability can be obtained as (30).

D. PROOF OF (31)

According to (29), we can bound the truncation error $|\epsilon_T|$ with the number of terms T as

$$
\begin{aligned}
&|\epsilon_T| \\
&= \sqrt{2\nu}e^{\nu} \sum_{k=T+1}^{\infty} W_{-k-\frac{1}{2},0}(2\nu)\gamma\left(k+1, \frac{\rho_t}{\sigma_{sr}^2\bar{\rho}}\right) \\
&\overset{(a)}{=} 2\nu \sum_{k=T+1}^{\infty} \frac{1}{k!} \int_0^{\infty} \frac{e^{-2\nu x}x^k}{(1+x)^{k+1}}dx \int_0^{\frac{\rho_t}{\sigma_{sr}^2\bar{\rho}}} e^{-y}y^k dy \\
&\overset{(b)}{=} \frac{2\nu}{(T+1)!} \int_0^{\infty} \int_0^{\frac{\rho_t}{\sigma_{sr}^2\bar{\rho}}} \frac{e^{-2\nu x}x^{T+1}}{(1+x)^{T+2}} e^{-y}y^{T+1} \\
&\qquad \times {}_1F_1\left(1; T+2; \frac{xy}{x+1}\right) dydx \\
&\overset{(c)}{=} \frac{2\nu}{T!} \int_0^{\infty} \int_0^{\frac{\rho_t}{\sigma_{sr}^2\bar{\rho}}} \frac{e^{-2\nu x}}{1+x} e^{-y} e^{\frac{xy}{x+1}} \\
&\qquad \times \gamma\left(T+1, \frac{xy}{x+1}\right) dydx \\
&\overset{(d)}{<} \frac{2\nu}{T!} \int_0^{\infty} \frac{e^{-2\nu x}}{1+x} dx \int_0^{\frac{\rho_t}{\sigma_{sr}^2\bar{\rho}}} \gamma(T+1, y)dy \\
&= \frac{2\nu}{T!}\Psi(1,1;2\nu)\left[\frac{\rho_t}{\sigma_{sr}^2\bar{\rho}}\gamma\left(T+1, \frac{\rho_t}{\sigma_{sr}^2\bar{\rho}}\right)\right. \\
&\qquad \left. -\gamma\left(T+2, \frac{\rho_t}{\sigma_{sr}^2\bar{\rho}}\right)\right],
\end{aligned}
$$

where $\nu = \frac{\sigma_{sr}^2}{2\eta^2\sigma_{si}^2\sigma_{ir}^2}$, (a) follows from [18, eq. (9.222.1)] and [18, eq. (8.350.1)], (b) follows by setting $j = k - T - 1$ and leveraging the series representation of Hypergeometric function [18, eq. (9.210.1)], (c) follows with the following equation

$$
\begin{aligned}
{}_1F_1\left(1; T+2; \frac{xy}{x+1}\right) &= (T+1)\left(\frac{xy}{x+1}\right)^{-(T+1)} e^{\frac{xy}{x+1}} \\
&\quad \times \gamma\left(T+1, \frac{xy}{x+1}\right),
\end{aligned}
$$

(d) follows as $\frac{x}{x+1} < 1$ for $x > 0$, and $\Psi(\cdot,\cdot;\cdot)$ is the confluent hypergeometric function [18, eq. (9.211.4)].

REFERENCES

[1] A. Al-Fuqaha, M. Guizani, M. Mohammadi, M. Aledhari, and M. Ayyash, "Internet of Things: A survey on enabling technologies, protocols, and applications," *IEEE Commun. Surveys Tuts.*, vol. 17, no. 4, pp. 2347–2376, 4th Quart., 2015.

[2] V. Liu, A. Parks, V. Talla, S. Gollakota, D. Wetherall, and J. R. Smith, "Ambient backscatter: Wireless communication out of thin air," in *Proc. ACM Special Interest Group Data Commun. (SIGCOMM)*, Hong Kong, 2013, pp. 39–50.

[3] A. N. Parks, A. Liu, S. Gollakota, and J. R. Smith, "Turbocharging ambient backscatter communication," in *Proc. ACM Special Interest Group Data Commun. (SIGCOMM)*, Chicago, IL, USA, 2014, pp. 619–630.

[4] B. Kellogg, A. Parks, S. Gollakota, J. R. Smith, and D. Wetherall, "Wi-Fi backscatter: Internet connectivity for RF-powered devices," in *Proc. ACM Special Interest Group Data Commun. (SIGCOMM)*, Chicago, IL, USA, 2014, pp. 607–618.

[5] D. Kuester and Z. Popovic, "How good is your tag?: RFID backscatter metrics and measurements," *IEEE Microw. Mag.*, vol. 14, no. 5, pp. 47–55, Jul. 2013.

[6] N. Van Huynh, D. T. Hoang, X. Lu, D. Niyato, P. Wang, and D. I. Kim. (Dec. 2017). "Ambient backscatter communications: A contemporary survey." [Online]. Available: https://arxiv.org/abs/1712.04804

[7] X. Lu, H. Jiang, D. Niyato, D. I. Kim, and Z. Han, "Wireless-powered device-to-device communications with ambient backscattering: Performance modeling and analysis," *IEEE Trans. Wireless Commun.*, vol. 17, no. 3, pp. 1528–1544, Mar. 2018.

[8] G. Yang, Y.-C. Liang, and Q. Zhang, "Cooperative receiver for ambient backscatter communications with multiple antennas," in *Proc. IEEE Int. Conf. Commun. (ICC)*, Paris, France, May 2017, pp. 1–6.

[9] G. Wang, F. Gao, R. Fan, and C. Tellambura, "Ambient backscatter communication systems: Detection and performance analysis," *IEEE Trans. Commun.*, vol. 64, no. 11, pp. 4836–4846, Nov. 2016.

[10] J. Qian, F. Gao, G. Wang, S. Jin, and H. Zhu, "Noncoherent detections for ambient backscatter system," *IEEE Trans. Wireless Commun.*, vol. 16, no. 3, pp. 1412–1422, Mar. 2017.

[11] D. Darsena, G. Gelli, and F. Verde, "Modeling and performance analysis of wireless networks with ambient backscatter devices," *IEEE Trans. Commun.*, vol. 65, no. 4, pp. 1797–1814, Jan. 2017.

[12] X. Kang, Y.-C. Liang, and J. Yang, "Riding on the primary: A new spectrum sharing paradigm for wireless-powered IoT devices," in *Proc. IEEE Int. Conf. Commun. (ICC)*, Paris, France, May 2017, pp. 1–6.

[13] Y. Zhang, J. Qian, F. Gao, and G. Wang, "Outage probability for ambient backscatter system with real source," in *Proc. IEEE Int. Workshop Signal Process. Adv. Wireless Commun. (SPAWC)*, Sapporo, Japan, Jul. 2017, pp. 1–5.

[14] W. Zhao, G. Wang, S. Atapattu, C. Tellambura, and H. Guan, "Outage analysis of ambient backscatter communication systems," *IEEE Commun. Lett.*, submitted.

[15] R. Long, G. Yang, Y. Pei, and R. Zhang, "Transmit beamforming for cooperative ambient backscatter communication systems," in *Proc. IEEE Global Telecommn. Conf. (GLOBECOM)*, Singapore, Dec. 2017, pp. 1–6.

[16] W. Zhao, G. Wang, F. Gao, Y. Zou, and S. Atapattu, "Channel capacity and lower bound for ambient backscatter communication systems," in *Proc. Int. Conf. Wireless Commun. Signal Process. (WCSP)*, Nanjing, China, 2017, pp. 1–6.

[17] T. M. Cover and J. A. Thomas, *Elements of Information Theory*. New York, NY, USA: Wiley, 2012.

[18] I. S. Gradshteyn and I. M. Ryzhik, *Table of Integrals, Series and Products*, 7th ed. San Francisco, CA, USA: Academic, 2007.

[19] T. Betlehem and A. J. Coulson, "Distribution of the sum of a complex Gaussian and the product of two complex Gaussians," in *Proc. Austral. Commun. Theory Workshop (AusCTW)*, Wellington, New Zealand, 2012, pp. 126–129.

[20] M. K. Simon and M.-S. Alouini, *Digital Communication Over Fading Channels*. New York, NY, USA: Wiley, 2005.

WENJING ZHAO received the B.Eng. degree in computer science and technology from Beijing Jiaotong University, Beijing, China, in 2016, where she is currently pursuing the Ph.D. degree with the Department of Computer Science and Technology. Her research interests include Internet of Things, performance analysis, signal processing technologies, and machine learning.

GONGPU WANG received the B.Eng. degree in communication engineering from Anhui University, Hefei, Anhui, China, in 2001, the M.Sc. degree from the Beijing University of Posts and Telecommunications, Beijing, China, in 2004, and the Ph.D. degree from the University of Alberta, Edmonton, Canada, in 2011. From 2004 to 2007, he was an Assistant Professor with the School of Network Education, Beijing University of Posts and Telecommunications. He is currently an Associate Professor with the School of Computer and Information Technology, Beijing Jiaotong University, China. His research interests include wireless communication theory, signal processing technologies, and Internet of Things.

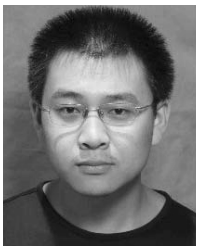

RONGFEI FAN received the B.E. degree in electrical engineering from the Harbin Institute of Technology, Harbin, China, in 2007, and the Ph.D. degree in electrical engineering from the University of Alberta, Edmonton, AB, Canada, in 2012. Since 2013, he has been a Faculty Member with the Beijing Institute of Technology, Beijing, China, where he is currently an Assistant Professor with the School of Information and Electronics. His research interest includes cognitive radio, cross-layer design, radio resource management for wireless communications, and energy harvesting.

LI-SHENG FAN received the bachelor's degree from the Department of Electronic Engineering, Fudan University, China, in 2002, the master's degree from the Department of Electronic Engineering, Tsinghua University, China, in 2005, and the Ph.D. degree from the Department of Communications and Integrated Systems, Tokyo Institute of Technology, Japan, in 2008. He is currently a Professor with Guangzhou University. His research interests span in the areas of wireless cooperative communications, physical-layer secure communications, interference modeling, and system performance evaluation. He has published many papers in international journals such as the IEEE TRANSACTIONS ON WIRELESS COMMUNICATIONS, the IEEE TRANSACTIONS ON COMMUNICATIONS, the IEEE TRANSACTIONS ON INFORMATION THEORY, and papers in conferences such as the IEEE ICC, the IEEE GLOBECOM, and the IEEE WCNC. He has also served as a member of Technical Program Committees for the IEEE conferences such as GLOBECOM, ICC, WCNC, and VTC. He is a Guest Editor of the *EURASIP Journal on Wireless Communications and Networking*, and served as the Chair of Wireless Communications and Networking Symposium for Chinacom 2014.

SAMAN ATAPATTU (M'14) received the B.Sc. degree in electrical and electronics engineering from the University of Peradeniya, Peradeniya, Sri Lanka, in 2003, the M.Eng. degree in telecommunications from the Asian Institute of Technology, Bangkok, Thailand, in 2007, and the Ph.D. degree in electrical engineering from the University of Alberta, Edmonton, AB, Canada, in 2013. He is currently a Research Fellow with the Department of Electrical and Electronic Engineering, The University of Melbourne, VIC, Australia. His general research interests include wireless communications and signal processing. He was a recipient of the 2016 Australian Research Councils Discovery Early Career Research Award.